Kinematic and Dynamic Modeling of a Parallel Manipulator with Eight Actuation Modes

Stéphane Caro, Damien Chablat, Philippe Wenger, Xianwen Kong

Kinematic and Dynamic Modeling of a Parallel Manipulator with Eight Actuation Modes

Stéphane Caro[1], Damien Chablat[1], Philippe Wenger[1] and Xianwen Kong[2]

[1]*Institut de Recherche en Communications et Cybernétique de Nantes, France, e-mail: {stephane.caro, damien.chablat, philippe.wenger}@irccyn.ec-nantes.fr*
[2]*School of Engineering and Physical Sciences, Heriot-Watt University, Edinburgh, UK, EH14 4AS, e-mail: X.Kong@hw.ac.uk*

Abstract. Kinematic and dynamic performances of parallel manipulators are usually not homogeneous throughout their operational workspace. This problem is usually solved by introducing actuation redundancy, which involves force control algorithms. Another approach is the selection of the best actuation modes along a trajectory to be followed with regard to the kinetostatic, elastostatic and dynamic performances of the parallel manipulator. Accordingly, this paper introduces a novel three degree-of-freedom planar parallel manipulator with variable actuation modes, named NAVARO. NAVARO stands for NAntes Variable Actuation RObot and has eight actuation modes. First, the prototype of the manipulator is presented. Then, its transmission systems are presented. Finally, the kinematic and dynamic models of the NAVARO are developed.

1 Introduction

A drawback of serial and parallel mechanisms is the inhomogeneity of the kinetostatic performance within their workspace. For instance, dexterity, accuracy and stiffness are usually bad in the neighbourhood of singularities that can appear in the workspace of such mechanisms. As far as the parallel mechanisms are concerned, their inverse kinematics problem (IKP) has usually many solutions, which correspond to the *working modes* of the mechanism [4]. Nevertheless, it is difficult to come up with a large operational workspace free of singularity with a given working mode. Consequently, a trajectory planning may require a change of the working mode by means of an alternative trajectory in order to avoid singular configurations. In such a case, the initial trajectory would not be followed. The common approach to solve this problem is to introduce actuation redundancy, that involves force control algorithms [1]. Another approach is to use the concept of joint-coupling as proposed by [11] or to select the actuated joint in each limb with regard to the pose of the moving-platform, [2].

In this paper, a three degree-of-freedom planar parallel manipulator with variable actuation modes, named NAVARO, is introduced. NAVARO stands for NAntes Variable Actuation RObot and has eight actuation modes. First, the prototype of the

manipulator is presented. Then, its transmission systems are presented. Finally, the kinematic and dynamic models of the NAVARO are developed.

2 Mechanism architecture

The concept of *variable actuated mechanism* (VAM) was introduced in [2, 11]. Indeed, they derived a VAM from the architecture of the 3-RPR planar parallel manipulator (PPM) by actuating either the first revolute joint or the prismatic joint of its limbs. This paper deals with the study of a VAM introduced in [10] and illustrated

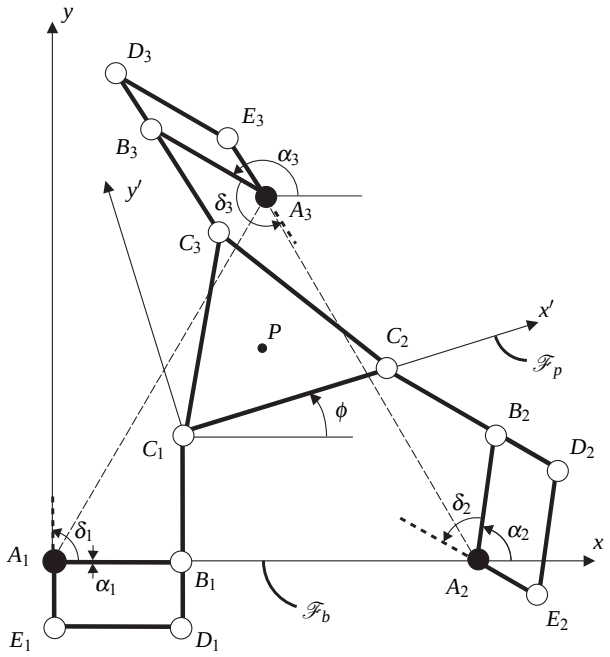

Fig. 1 3-RRR PPM with variable actuation

in Fig. 1. This mechanism is derived from the architecture of the 3-RRR PPM. The first link of each limb of the conventional 3-RRR manipulator is replaced by parallelogram $A_iB_iD_iE_i$ to come up with the mechanism at hand. Accordingly, links A_iB_i and B_iC_i can be driven independently, i.e., angles α_i and δ_i are actuated and uncoupled, by means of an actuator and a transmission system, mounted to the base and located in point A_i, $i = 1,2,3$.

It turns out that the VAM has eight *actuating modes* as shown in Table 1. Indeed, the actuating mode of the mechanism depends on its actuated joints. For instance, the first actuating mode corresponds to the 3-RRR mechanism, also called

$\underline{R}RR_1$-$\underline{R}RR_2$-$\underline{R}RR_3$ mechanism in the scope of this paper, as the first revolute joints (located at point A_i) of its limbs are actuated. Likewise, the eighth actuating mode corresponds to the 3-R$\underline{R}$R manipulator, also called $R\underline{R}R_1$-$R\underline{R}R_2$-$R\underline{R}R_3$ mechanism, as the second revolute joints (located at point B_i) of its limbs are actuated.

The moving platform pose of the VAM is determined by means of the Cartesian coordinates (x,y) of operation point P expressed in the base frame $\mathscr{F}_b$ and angle ϕ, namely, the angle between frames $\mathscr{F}_b$ and $\mathscr{F}_p$. Moreover, the passive and actuated joints do not have any stop. Points A_1, A_2 and A_3, (C_1, C_2 and C_3, respectively) lie at the corners of an equilateral triangle, of which the geometric center is point O (point P, resp.).

Table 1 The eight actuating modes of the NAVARO

Actuating mode number		driven links	active angles
1	$\underline{R}RR_1$-$\underline{R}RR_2$-$\underline{R}RR_3$	A_1B_1, A_2B_2, A_3B_3	α_1, α_2, α_3
2	$\underline{R}RR_1$-$\underline{R}RR_2$-$R\underline{R}R_3$	A_1B_1, A_2B_2, A_3E_3	α_1, α_2, δ_3
3	$\underline{R}RR_1$-$R\underline{R}R_2$-$\underline{R}RR_3$	A_1B_1, A_2E_2, A_3B_3	α_1, δ_2, α_3
4	$R\underline{R}R_1$-$\underline{R}RR_2$-$\underline{R}RR_3$	A_1E_1, A_2B_2, A_3B_3	δ_1, α_2, α_3
5	$\underline{R}RR_1$-$R\underline{R}R_2$-$R\underline{R}R_3$	A_1B_1, A_2E_2, A_3E_3	α_1, δ_2, δ_3
6	$R\underline{R}R_1$-$R\underline{R}R_2$-$\underline{R}RR_3$	A_1E_1, A_2E_2, A_3B_3	δ_1, δ_2, α_3
7	$R\underline{R}R_1$-$\underline{R}RR_2$-$R\underline{R}R_3$	A_1E_1, A_2B_2, A_3E_3	δ_1, α_2, δ_3
8	$R\underline{R}R_1$-$R\underline{R}R_2$-$R\underline{R}R_3$	A_1E_1, A_2E_2, A_3E_3	δ_1, δ_2, δ_3

Fig. 2 The NAVARO prototype

Figure 2 shows the prototype of the NAVARO, which has been developed at IRCCyN[1].

[1] IRCCyN: Institut de Recherche en Communications et Cybernétique de Nantes

3 Transmission system

A transmission system has been developed and mounted in each leg of the NAVARO in order for the manipulator to be able to switch smoothly from one actuation mode to another along a prescribed trajectory. Figure 3 illustrates a CAD modeling of the

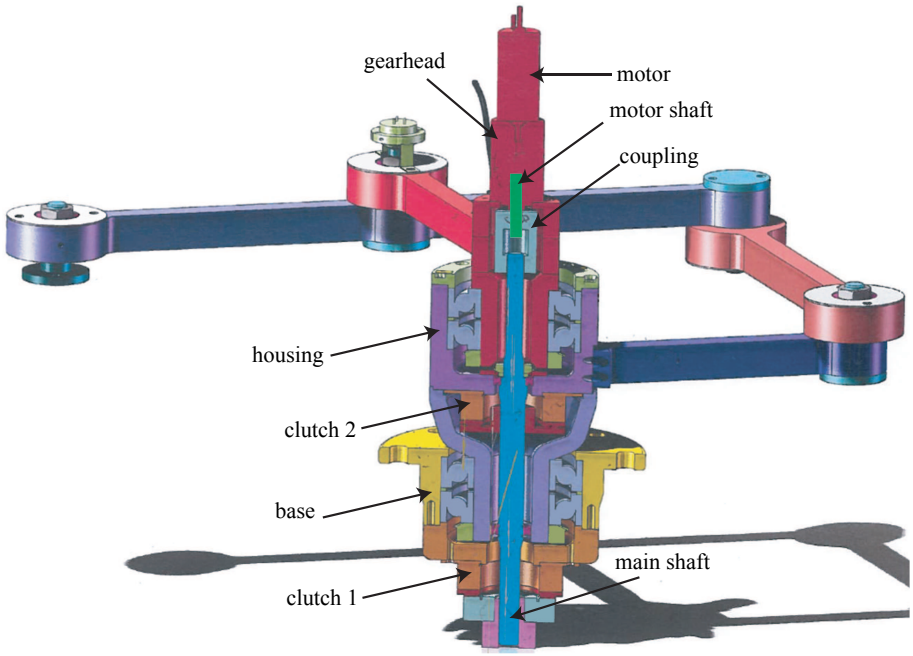

Fig. 3 The NAVARO transmission system

transmission system of the NAVARO. This system can be seen as a double clutch system and contains: (*i*) a motor; (*ii*) a gearhead, (*iii*) a motor shaft, (*iv*) a main shaft (in cyan), (*v*) a base (in yellow), (*vi*) a housing (in purple) and (*vii*) two clutches (in brown). As a matter of fact, the two clutches 1 and 2 are electromagnetic brakes.

Each transmission system has four actuation schemes that are def ned thereafter:

1. **None of clutches 1 and 2 are active**: The main shaft is free to move with respect to the housing and the base. In that case, none of the f rst two revolute joints of the corresponding legs are actuated, namely, angles α_i and δ_i are passive, $i = 1,2,3$.
2. **Clutch 1 is active while Clutch 2 is not**: The main shaft is f xed with respect to the base, i.e., the link A_iB_i is driven thanks to the rotation of the motor shaft. In that case, angle α_i is active and angle δ_i is passive, $i = 1,2,3$.
3. **Clutch 2 is active while Clutch 1 is not**: The main shaft is attached to the housing, but is free to move with respect to the base. In that case, angle α_i is passive and angle δ_i is active, $i = 1,2,3$.

4. **Both clutches 1 and 2**: The blue shaft is attached to both the base and the housing. It means that the housing cannot move and link A_iE_i is fixed. In that case, link C_iD_i performs a circular translation with respect to point A_i, $i = 1,2,3$. This actuation scheme amounts to an actuated Π joint[2].

Only the second and third actuation schemes of each transmission system are used in the NAVARO prototype in order to keep the three degrees of freedom motion of the moving-platform and to avoid any actuation redundancy and under-actuation. However, it is noteworthy that the NAVARO behaves like a five-bar mechanism when the fourth actuation scheme of the transmission system is used in one leg, the second or the third actuation scheme is used in one of the other two legs two and the first actuation scheme is used in the third leg.

4 Kinematic analysis of the NAVARO

4.1 Kinematic modeling

The velocity $\dot{\mathbf{p}}$ of point P can be obtained in three different forms, depending on which leg is traversed, namely,

$$\dot{\mathbf{p}} = \dot{\alpha}_1\mathbf{E}(\mathbf{c}_1 - \mathbf{a}_1) + \dot{\delta}_1\mathbf{E}(\mathbf{c}_1 - \mathbf{b}_1) + \dot{\phi}\mathbf{E}(\mathbf{p} - \mathbf{c}_1) \tag{1}$$

$$\dot{\mathbf{p}} = \dot{\alpha}_2\mathbf{E}(\mathbf{c}_2 - \mathbf{a}_2) + \dot{\delta}_2\mathbf{E}(\mathbf{c}_2 - \mathbf{b}_2) + \dot{\phi}\mathbf{E}(\mathbf{p} - \mathbf{c}_2) \tag{2}$$

$$\dot{\mathbf{p}} = \dot{\alpha}_3\mathbf{E}(\mathbf{c}_3 - \mathbf{a}_3) + \dot{\delta}_3\mathbf{E}(\mathbf{c}_3 - \mathbf{b}_3) + \dot{\phi}\mathbf{E}(\mathbf{p} - \mathbf{c}_3) \tag{3}$$

with matrix $\mathbf{E}$ defined as

$$\mathbf{E} = \begin{bmatrix} 0 & -1 \\ 1 & 0 \end{bmatrix}$$

$\mathbf{a}_i$, $\mathbf{b}_i$ and $\mathbf{c}_i$ are the position vectors of points A_i, B_i and C_i, respectively. $\dot{\alpha}_i$, $\dot{\delta}_i$ and $\dot{\phi}$ are the rates of angles α_i, δ_i and ϕ depicted in Fig. 1, $i = 1,2,3$.

The kinematic model of the VAM under study can be obtained from Eqs.(1)-(c) by eliminating the idle joint rates. However, the latter depend on the actuating mode of the mechanism. For instance, $\dot{\delta}_1$, $\dot{\delta}_2$ and $\dot{\delta}_3$ are idle with the first actuating mode and the corresponding kinematic model is obtained by dot-multiplying Eqs.(1)-(c) with $(\mathbf{c}_i - \mathbf{b}_i)^T$, $i = 1,2,3$. Likewise, $\dot{\delta}_1$, $\dot{\delta}_2$ and $\dot{\alpha}_3$ are idle with the second actuating mode and the corresponding kinematic model is obtained by dot-multiplying Eqs.(1)-(b) with $(\mathbf{c}_i - \mathbf{b}_i)^T$, $i = 1,2$, and Eq.(3) with $(\mathbf{c}_3 - \mathbf{a}_3)^T$.

The kinematic model of the VAM can now be cast in vector form, namely,

$$\mathbf{A}\mathbf{t} = \mathbf{B}\dot{\mathbf{q}} \quad \text{with} \qquad \mathbf{t} = [\dot{\mathbf{p}}\ \dot{\phi}]^T \quad \text{and} \quad \dot{\mathbf{q}} = [\dot{q}_1\ \dot{q}_2\ \dot{q}_3]^T \tag{4}$$

[2] A Π joint is also called parallelogram joint [3]

with $\dot{\mathbf{q}}$ thus being the vector of actuated joint rates. $\dot{q}_i = \dot{\alpha}_i$ when link A_iB_i is driven and $\dot{q}_i = \dot{\delta}_i$ when link A_iE_i is driven, $i = 1,2,3$. $\mathbf{A}$ and $\mathbf{B}$ are respectively, the direct and the inverse Jacobian matrices of the mechanism, def ned as

$$\mathbf{A} = \begin{bmatrix} (\mathbf{c}_1 - \mathbf{h}_1)^T & -(\mathbf{c}_1 - \mathbf{h}_1)^T \mathbf{E}(\mathbf{p} - \mathbf{c}_1) \\ (\mathbf{c}_2 - \mathbf{h}_2)^T & -(\mathbf{c}_2 - \mathbf{h}_2)^T \mathbf{E}(\mathbf{p} - \mathbf{c}_2) \\ (\mathbf{c}_3 - \mathbf{h}_3)^T & -(\mathbf{c}_3 - \mathbf{h}_3)^T \mathbf{E}(\mathbf{p} - \mathbf{c}_3) \end{bmatrix} \tag{5}$$

$$\mathbf{B} = \text{diag}\left[(\mathbf{c}_i - \mathbf{b}_i)^T \mathbf{E}(\mathbf{b}_i - \mathbf{a}_i)\right], \quad i = 1,2,3 \tag{6}$$

where $\mathbf{h}_i = \mathbf{b}_i$ when link A_iB_i is driven and $\mathbf{h}_i = \mathbf{a}_i$ when link B_iC_i is driven, $i = 1,2,3$.

When $\mathbf{A}$ is non singular, we obtain the relation

$$\mathbf{t} = \mathbf{J}_p \dot{\mathbf{q}} \quad \text{with} \quad \mathbf{J}_p = \mathbf{A}^{-1}\mathbf{B} \tag{7}$$

Likewise, we obtain

$$\dot{\mathbf{q}} = \mathbf{K}_p \, \mathbf{t} \tag{8}$$

when $\mathbf{B}$ is non singular with $\mathbf{K}_p$ denoting the inverse of $\mathbf{J}_p$.

4.2 Singularity analysis

The singular conf gurations associated with the direct-kinematic matrix of PPMs are well known [9]. For the 3-RRR PPM, such conf gurations are reached whenever lines (B_1C_1), (B_2C_2) and (B_3C_3) intersect (possibly at inf nity). For the 3-RRR PPM, such conf gurations are reached whenever lines (A_1C_1), (A_2C_2) and (A_3C_3) intersect. Consequently, the singular conf gurations associated with the direct-kinematic matrix of the NAVARO are reached whenever lines (H_1C_1), (H_2C_2) and (H_3C_3) intersect where H_i stands for B_i (A_i, resp.) when link A_iB_i (B_iC_i, resp.) is driven, $i = 1,2,3$.

From Eq.(6), the singular conf gurations associated with the inverse-kinematics of the NAVARO are reached whenever points A_i, B_i, and C_i are aligned.

5 Dynamic modeling of the NAVARO

The inverse dynamic model of a robot provides its joint torques and forces as a function of the joint positions and its time derivatives. The direct dynamic model gives the joint accelerations as a function of joint positions, velocities and torques. Different approaches such as virtual work principle, Lagrange formalism and Newton Euler equations have been adopted in the literature [9]. Here the method developed in [6] is used to derive the dynamic model of the NAVARO. In [6], the dynamic models of the legs are obtained with classical methods used for serial robots, while

the dynamic model of the platform is obtained with Newton-Euler equations. Then, they are projected onto the actuated joint axes by means of Jacobian matrices. It is noteworthy that the legs of the NAVARO contain some closed loop chains contrary to the legs of the parallel manipulators analyzed in [6]. As a consequence, the methodology presented in [6] used to express the dynamic modeling of parallel manipulators is improved in this paper in order to be suitable for the dynamic modeling of the NAVARO. One diff culty lies in the choice of the joint to be cut to come up with an appropriate tree structure of the NAVARO for its dynamic modeling as explained thereafter.

5.1 Inverse dynamic model

To project the dynamics of the legs onto the active joint space, the Jacobian between the two spaces is used. The projection of the platform dynamics is performed by multiplying the expression with the transpose of the kinematic Jacobian matrix:

$$\Gamma = \mathbf{J}_p^T \mathbf{F}_p + \sum_{i=1}^{m} \left(\frac{\partial \dot{\mathbf{q}}_i}{\partial \dot{\mathbf{q}}_a} \right)^T \mathbf{H}_i \tag{9}$$

where $\mathbf{J}_p$ is the kinematic Jacobian matrix of the robot def ned by Eq. (7), $\mathbf{F}_p$ contains the total forces and moments applied on the platform, $\dot{\mathbf{q}}_a$ is the vector of active joint velocities and $\mathbf{H}_i$ is the inverse dynamic model of the ith leg. The following relationship holds:

$$\left(\frac{\partial \dot{\mathbf{q}}_i}{\partial \dot{\mathbf{q}}_a} \right) = \mathbf{J}_i^{-1} \mathbf{J}_{vi} \mathbf{J}_p \tag{10}$$

Matrix $\mathbf{J}_i$ is the Jacobian matrix of leg i ($i = 1, \ldots, m$, being m the number of legs), $\mathbf{J}_{vi}$ is the matrix that maps the velocity $\mathbf{v}_i$ of the ith leg into the moving platform twist $\mathbf{t}_p$:

$$\mathbf{v}_i = \mathbf{J}_i \dot{\mathbf{q}}_i \tag{11}$$

$$\mathbf{v}_i = \mathbf{J}_{vi} \mathbf{t}_p \tag{12}$$

As the active joint variables are independent, Eq. (9) is rewritten as:

$$\Gamma = \mathbf{H}^a + \mathbf{J}_p^T \left(\mathbf{F}_p + \sum_{i=1}^{m} \mathbf{J}_{vi}^T \mathbf{J}_i^{-T}(:, p_i) \mathbf{H}_i^p \right) \tag{13}$$

where $\mathbf{H}^a$ is the vector of active torques of the legs and index p_i of matrix $\mathbf{J}_i^{-T}$ refers to the passive joint variable number.

Each leg of the NAVARO contains a parallelogram closed loop and their dynamics should be f rst computed. Accordingly, the loop is opened and its equivalent tree structure is analyzed. The open loop is described using the Modif ed Denavit

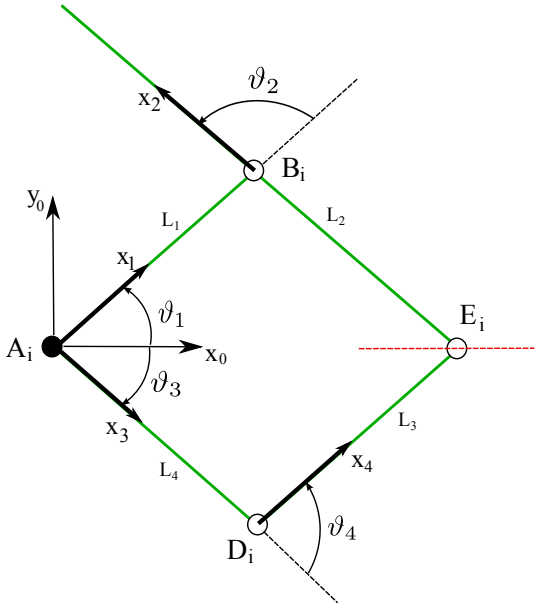

Fig. 4 Geometric model of the equivalent tree structure of the leg of the NAVARO

Hartenberg parameters [7] as illustrated in Fig. 4, where the cut joint is located at point E_i and highlighted by the red dotted line. The parameters are given in Table 2.

j	$a(j)$	σ_j	γ_j	b_j	α_j	d_j	ϑ_j	r_j
1	0	0	0	0	0	0	ϑ_1	0
2	1	0	0	0	0	L_1	ϑ_2	0
3	0	0	0	0	0	0	ϑ_3	0
4	3	0	0	0	0	L_4	ϑ_4	0

Table 2 Modif ed Denavit-Hartenberg parameters of the equivalent tree structure of one leg of the NAVARO

The dynamic model of the equivalent tree structure is def ned as:

$$\Gamma_{tr,i} = \mathbf{A}_{tr,i}\ddot{\mathbf{q}}_i + \mathbf{h}_{tr,i} = \begin{bmatrix} \Gamma_{i1} \\ \Gamma_{i2} \\ \Gamma_{i3} \\ \Gamma_{i4} \end{bmatrix} \tag{14}$$

with

$$\ddot{\mathbf{q}}_i = \begin{bmatrix} \ddot{q}_{i1} \\ \ddot{q}_{i2} \\ \ddot{q}_{i3} \\ \ddot{q}_{i4} \end{bmatrix} \tag{15}$$

Once the dynamic model of the open loop is computed, it is projected onto the closed loop in order to obtain the torques $\mathbf{H}_i$ of the ith leg:

$$\mathbf{H}_i = \mathbf{P}^T \Gamma_{tr,i} = \left(\frac{\partial \mathbf{q}_i}{\partial \mathbf{q}_{ai}} \right)^T \Gamma_{tr,i} = \begin{bmatrix} H_{i1} \\ H_{i2} \end{bmatrix} \tag{16}$$

The joint angle vector is expressed as:

$$\mathbf{q}_i = \begin{bmatrix} q_{i1} \\ q_{i2} \\ q_{i3} \\ q_{i4} \end{bmatrix} = \begin{bmatrix} \vartheta_1 \\ \vartheta_2 \\ \vartheta_3 \\ \vartheta_4 \end{bmatrix} \tag{17}$$

The passive joint angles ϑ_3 and ϑ_4 are def ned as a function of angles ϑ_1 and ϑ_2 as follows:

$$\begin{aligned} \vartheta_3 &= -\pi + \vartheta_1 + \vartheta_2 \\ \vartheta_4 &= \pi - \vartheta_2 \end{aligned} \tag{18}$$

Therefore, the projection matrix $\mathbf{P}$ is def ned as:

$$\mathbf{P} = \left(\frac{\partial \mathbf{q}_i}{\partial \mathbf{q}_{ai}} \right) = \begin{bmatrix} 1 & 0 \\ 0 & 1 \\ 1 & 1 \\ 0 & -1 \end{bmatrix} \tag{19}$$

The platform dynamics is calculated following the Newton-Euler equations and is def ned for the general case as:

$$\mathbf{F}_p = \mathbb{J}_p \begin{bmatrix} \dot{\mathbf{v}}_P - \mathbf{g} \\ \dot{\omega}_p \end{bmatrix} + \begin{bmatrix} \omega_p \times (\omega_p \times \mathbf{MS}_p) \\ \omega_p \times (\mathbf{I}_p \omega_p) \end{bmatrix} \tag{20}$$

where $\mathbf{MS}_p$ is the vector of f rst moments of the platform around the origin of the platform frame:

$$\mathbf{MS}_p = [MX_p \quad MY_p \quad MZ_p]^T \tag{21}$$

$\mathbb{J}_p$ is the spatial inertia matrix of the platform:

$$\mathbb{J}_p = \begin{bmatrix} M_p \mathbf{I}_3 & -\hat{\mathbf{MS}}_p \\ \hat{\mathbf{MS}}_p & \mathbf{I}_p \end{bmatrix} \tag{22}$$

$\mathbf{I}_p$ is the inertia matrix of the platform:

$$\mathbf{I}_p = \begin{bmatrix} XX_p & XY_p & XZ_p \\ YX_p & YY_p & YZ_p \\ ZX_p & ZY_p & ZZ_p \end{bmatrix} \tag{23}$$

$\hat{\mathbf{MS}}_p$ is the skew matrix associated with the vector $\mathbf{MS}_p$:

$$\hat{\mathbf{MS}}_p = \begin{bmatrix} 0 & -MZ_p & MY_p \\ MZ_p & 0 & -MX_p \\ -MY_p & MX_p & 0 \end{bmatrix} \tag{24}$$

Since the moving-platform of the NAVARO performs a planar motion, vector $\mathbf{MS}_p$ takes the form:

$$\mathbf{MS}_p = [MX_p \quad MY_p \quad 0]^T \tag{25}$$

and

$$\mathbf{I}_p = \begin{bmatrix} 0\,0 & 0 \\ 0\,0 & 0 \\ 0\,0 & ZZ_p \end{bmatrix} \tag{26}$$

Therefore, Eq. (9) becomes:

$$\Gamma = \mathbf{J}_r^T \mathbf{S}^T \mathbf{F}_p + \sum_{i=1}^{m} \left(\mathbf{J}_i^{-1} \mathbf{J}_{vi} \mathbf{S} \mathbf{J}_r \right)^T \mathbf{H}_i \tag{27}$$

5.2 Direct dynamic model

The direct dynamic model (DDyM) gives the platform Cartesian accelerations as a function of the Cartesian position and velocity of the platform and the motorized joint torques. In [6] it is shown that the direct dynamic model can be computed with the following general form:

$$\dot{\mathbf{t}}_r = \mathbf{A}_{robot}^{-1} \left(\mathbf{J}_r^{-T} \Gamma - \mathbf{h}_{robot} \right) \tag{28}$$

where $\mathbf{A}_{robot}$ is the total inertia matrix of the robot with respect to the Cartesian space, $\mathbf{h}_{robot}$ is a term that includes the Coriolis, centrifugal and gravity forces.

The inverse dynamic model of the *i*th leg is formulated as:

$$\mathbf{H}_i(\mathbf{q}_i, \dot{\mathbf{q}}_i, \ddot{\mathbf{q}}_i) = \mathbf{A}_i \ddot{\mathbf{q}}_i + \mathbf{h}_i(\mathbf{q}_i, \dot{\mathbf{q}}_i) \tag{29}$$

Upon differentiation of Eqs. (11) and (12) we obtain:

$$\dot{\mathbf{v}}_i = \mathbf{J}_i \ddot{\mathbf{q}}_i + \dot{\mathbf{J}}_i \dot{\mathbf{q}}_i \tag{30}$$

$$\dot{\mathbf{v}}_i = \dot{\mathbf{J}}_{vi} \mathbf{t}_p + \mathbf{J}_{vi} \dot{\mathbf{t}}_p \tag{31}$$

The joint accelerations in Eq. (29) are then substituted with:

$$\ddot{\mathbf{q}}_i = \mathbf{J}_i^{-1} \left(\dot{\mathbf{J}}_{vi} \mathbf{t}_p + \mathbf{J}_{vi} \dot{\mathbf{t}}_p - \dot{\mathbf{J}}_i \dot{\mathbf{q}}_\mathbf{i} \right) \tag{32}$$

For the NaVARo the leg inertia matrix $\mathbf{A}_{it}$ and the Coriolis, centrifugal and gravity torques $\mathbf{h}_{it}$ were f rst computed for the equivalent tree structure with SYMORO+

[8], then projected onto closed loop by means of the projection matrix **P** def ned by Eq. (19) to obtain $\mathbf{A}_i$ and $\mathbf{h}_i$:

$$\mathbf{A}_i = \mathbf{P}^T \mathbf{A}_{it} \mathbf{P} \tag{33}$$

$$\mathbf{h}_i = \mathbf{P}^T \mathbf{h}_{it} \tag{34}$$

Having all these elements, the robot platform acceleration is computed with Eq. (28).

5.3 Validation of the dynamic model

Both inverse and direct dynamic models of the NAVARO were implemented in Matlab. A model was realized in Simulink to simulate the behaviour of the dynamic model of the NAVARO in response to a test trajectory. The actuation mode is specif ed in the def nition of the trajectory in order to select the appropriate robot Jacobian during the computation of both inverse and direct dynamic models.

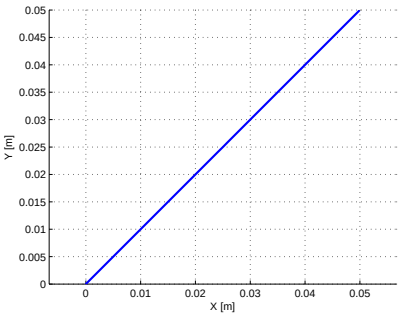

Fig. 5 Path of the test trajectory in the Cartesian space

Figure 5 illustrates the path of the test trajectory in the Cartesian space. Figure 6 shows the velocity and acceleration prof les of the test trajectory Figures 7 provides the required motor torques computed with the dynamic model of the NAVARO written in Matlab to follow the test trajectory with the 1st actuation mode of the NAVARO. Figure 8 depicts the position and linear acceleration errors of the moving platform along the test trajectory. The acceleration errors are of order 10^{-16}. The position errors are instead of order 10^{-4}. Considering that there are possible integration errors, those errors are acceptable. Finally, those results were also compared with those obtained with MapleSIM software and the correlation turned to be good.

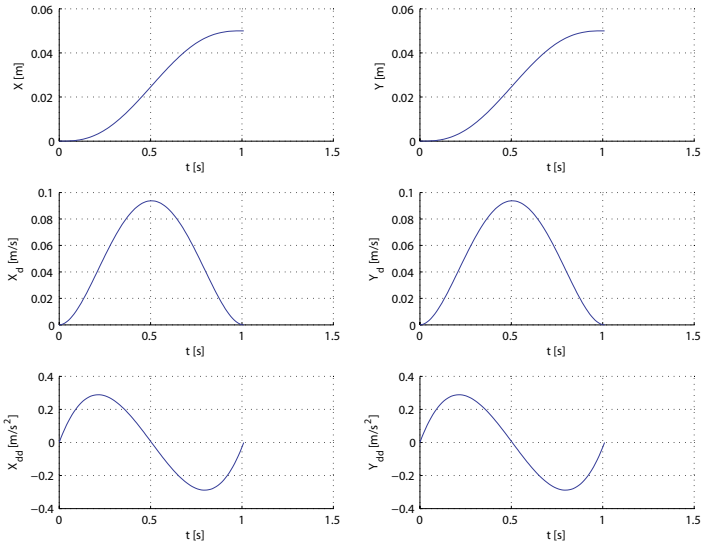

Fig. 6 Velocity and acceleration prof les of the test trajectory

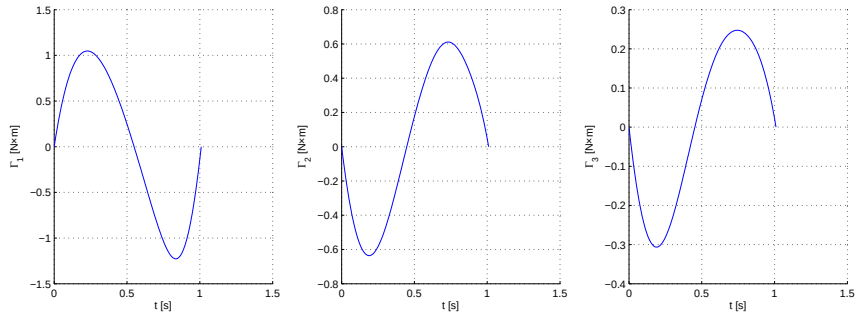

Fig. 7 Required motor torques to follow the test trajectory with the 1st actuation mode

6 Conclusions

In this paper, a three degree-of-freedom planar parallel manipulator with variable actuation modes, named NAVARO, was introduced. NAVARO stands for NAntes Variable Actuation RObot and has eight actuation modes. First, the prototype of the manipulator was presented. Then, its transmission systems were described. The kinematic and dynamic models of the NAVARO have also been developed. It is noteworthy that the legs of the NAVARO contain some closed loop chains contrary to the legs of the parallel manipulators analyzed in [6]. As a consequence, the methodology presented in [6] used to express the dynamic modeling of parallel manipulators has been improved to be suitable for the dynamic modeling of the NAVARO.

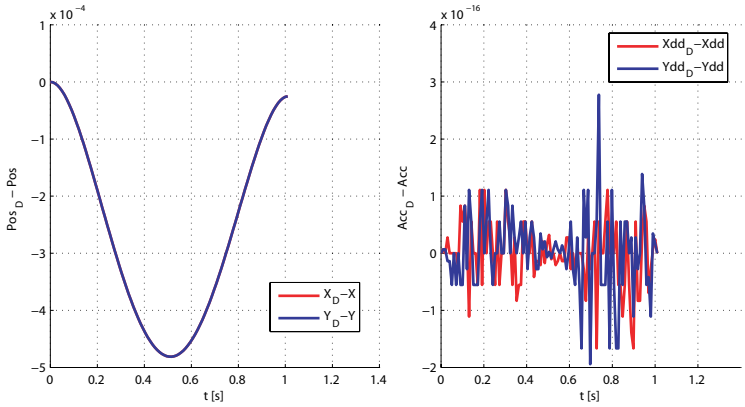

Fig. 8 Position and linear acceleration errors of the moving platform along the test trajectory

The development of an algorithm to deal with the actuation mode changing of the NAVARO and optimal path placement will be part of the future work. The kinematic and dynamic models will be also validated experimentally.

7 Acknowledgements

The firs three authors would like to acknowledge the financia support of the French "Agence Nationale de la Recherche" (Project "SiRoPa", SIngularités des RObots PArallèles). The authors would like to thank the Royal Society, United Kingdom, through an International Joint Project No. JP100715.
M. Iván Sáinz and Prof. Wisama Khalil are also acknowledged for their great help during the design of the double clutch system and the dynamic modeling of the NAVARO, respectively.

References

1. Alba-Gomez, O., Wenger, P. and Pamanes, A. (2005), Consistent Kinetostatic Indices for Planar 3-DOF Parallel Manipulators, Application to the Optimal Kinematic Inversion, *Proceedings of the ASME 2005 IDETC/CIE Conference*.
2. Arakelian, V., Briot, S. and Glazunov, V. (2007). Increase of Singularity-Free Zones in the Workspace of Parallel Manipulators Using Mechanisms of Variable Structure. *Mech. Mach. Theory*, Available online at www.sciencedirect.com.
3. Caro, S., Khan, W.A., Pasini, D. and Angeles, J. (2010), The Rule-based Conceptual Design of the Architecture of Serial Schönflies-motio Generators *Mechanism and Machine Theory*, vol. 45, no. 2, pp. 251–260.

4. Chablat, D. and Wenger, P. (1998), Working Modes and Aspects in Fully-Parallel Manipulator, *Proceeding IEEE International Conference on Robotics and Automation*, pp. 1964–1969, May.
5. Chablat, D., Wenger, P., Caro, S. and Angeles, J. (2002), The Isoconditioning Loci of Planar Three-DOF Parallel Manipulators, *Proc. DETC ASME*, Montreal, Canada.
6. Khalil, W. and Ibrahim, O. (2007) General solution for the dynamic modeling of parallel robots. *Journal of intelligent and robotic systems*, 49:19–37.
7. Khalil, W. and Dombre, E. (2004) *Modeling, Identification and Control Of Robots*. Elsevier Butterworth Heinemann.
8. Khalil, W. and Creusot, D. (1997) SYMORO+: A system for the symbolic modelling of robots. *Robotica*, 15:153–161.
9. Merlet, J-P. (2006), *Parallel robots*, Springer.
10. Rakotomanga, N., Chablat, D. and Caro, S. (2008), Performance of a Planar Parallel Mechanism with Variable Actuation, *Advances in Robot Kinematics*, Batz-sur-Mer, France, June 22-26, pp. 311–320.
11. Theingin, Chen, I.-M., Angeles, J. and Li, C. (2007), Management of parallel-manipulator singularities using joint-coupling *Advanced Robotics*, vol. 21, no. 5-6, pp. 583–600.